Journal of Alloys and Compounds 958 (2023) 170445

Contents lists available at ScienceDirect

Journal of Alloys and Compounds

journal homepage: www.elsevier.com/locate/jalcom

Research article

Structural and magnetic transitions in the $Bi_2Fe_4O_9/BiFeO_3$ composite

L.V. Udod [a,b,*], S.S. Aplesnin [a,b], M.N. Sitnikov [b], E.V. Eremin [a,b,c], M.S. Molokeev [a,c], A.V. Shabanov [a], O.B. Romanova [a], A.M. Kharkov [b]

[a] Kirensky Institute of Physics, Federal Research Center KSC SB RAS, 660036 Krasnoyarsk, Russia
[b] Reshetnev Siberian State University of Science and Technology, 660037 Krasnoyarsk, Russia
[c] Siberian Federal University, 660041 Krasnoyarsk, Russia

ARTICLE INFO

Article history:
Received 6 December 2022
Received in revised form 17 April 2023
Accepted 3 May 2023
Available online 5 May 2023

Keywords:
Composite materials
Magentisation
Optical properties
Scanning electron microscopy (SEM)
Ultrasonics
Phase transitions

ABSTRACT

A $Bi_2Fe_4O_9/BiFeO_3$ composite with a percentage ratio of 67/33 has been synthesized, its morphological analysis has been carried out. The average crystallite sizes for each phase have been determined. The magnetization hysteresis has been established and the temperature of its disappearance has been found. Using the infrared absorption spectra, temperatures of the magnetic phase transitions in each phase have been determined from the magnetic susceptibility, magnetostriction constant, ultrasound damping coefficient, and phonon mode softening. The change of magnetostriction constant sign observed in the vicinity of the spin reorientation transition and antiferromagnetic transition in mullite has been attributed to the change of the sign of the magnetoelastic constants. The interaction between the phases in the composite and the correlation of its structural and magnetic properties have been established.

1. Introduction

The combination of the ferroelectric and ferromagnetic or antiferromagnetic properties in materials is widely used in multifunctional memory and spintronic devices [1,2]. Bismuth ferrite $BiFeO_3$ belongs to multiferroics and is characterized by a strong coupling between the magnetic and ferroelectric subsystems [3] and high temperatures of the magnetic ($T_N \sim 643$ K) and ferroelectric ($T_C \sim 1083$ K) ordering [4]. At 140 K, the $BiFeO_3$ films undergo a surface structural transition without changing the crystal structure symmetry [5], which is accompanied by a dramatic change in the sample volume, an anomaly in the temperature dependence of the pyroelectric current, a conductivity maximum, and a singularity in the impedance spectrum. The $BiFeO_3$ crystal structure allows the coexistence of the antiferromagnetic and ferroelectric phases; however, this compound does not exhibit magnetoelectric effect due to the spatial modulation of its spin structure [6,7]. $BiFeO_3$ is rhombohedral (sp. gr. *R*3*c*). Oxygen octahedra in the bismuth ferrite crystal structure are rotated around the [111] axis without changing the space group, which is the reason of magnetic ordering [8]. Therefore, a necessary condition for observing the magnetoelectric effect is the suppression of the space modulated structure, which occurs in strong magnetic fields [7], when the system undergoes an incommensurate phase–commensurate phase transition between the spin-modulated and uniform antiferromagnetic states.

Mullite $Bi_2Fe_4O_9$ also belongs to the family of multiferroics [9,10]. In contrast to the $BiFeO_3$ compound, it is paramagnetic at room temperature and has an orthorhombic crystal structure (sp. gr. *Pbam*) [11]. Four Fe^{3+} ions hold two different positions in the $Bi_2Fe_4O_9$ structure: $Fe^{3+}(1)$ occupies the octahedral FeO_6 site and $Fe^{3+}(2)$ occupies the tetrahedral Fe_2O_7 site [12]. At $T = 264 \pm 3$ K, the bulk $Bi_2Fe_4O_9$ compound passes to the antiferromagnetic state. The magnetic moment of Fe^{3+} ions is $\mu_B = 4.95\ \mu_B$ [13] or, as was reported in [14], $\mu_B = 3.9–4.0\ \mu_B$. The magnetic properties of the polycrystalline $Bi_2Fe_4O_9$ compound depend from the synthesis technique used and crystallite size. The sample with a crystallite size of 200–450 nm synthesized using ethylenediaminetetraacetic acid [15] exhibits the weak magnetization at room temperature. The $Bi_2Fe_4O_9$ polycrystal with a micron grain size obtained by melting undergoes an antiferromagnetic phase transition at 250 K [16,17]. The polycrystalline $Bi_2Fe_4O_9$ ceramics with grains smaller than 200 nm is characterized by the room-temperature magnetic hysteresis, which vanishes upon heating [18]. The single-crystal $Bi_2Fe_4O_9$ samples have a N é el temperature of $T_N = 238$ K [12]. A critical grain size of 50 nm corresponding to the occurrence of the magnetization at room temperature was found in the $Bi_2Fe_4O_9$ compound synthesized by glycine combustion method [19].

* Correspondence to: Akademgorodok 50, bld. 38, Krasnoyarsk 660036, Russia.
E-mail address: luba@iph.krasn.ru (L.V. Udod).

https://doi.org/10.1016/j.jallcom.2023.170445
0925-8388/

The $Bi_2(Sn_{0.7}Fe_{0.3})_2O_7/Bi_2Fe_4O_9$ composite with a low (9%) mullite content exhibits weak ferromagnetism [20]. The remanent magnetization of $Bi_2Fe_4O_9$ in the oxygen-deficient $Bi_2(Sn_{0.7}Fe_{0.3})_2O_7$ matrix is higher than that of the pure $Bi_2Fe_4O_9$ polycrystal by an order of magnitude. The magnetic hysteresis in the $Bi_2(Sn_{0.7}Fe_{0.3})_2O_7/Bi_2Fe_4O_9$ composite and the absence of saturation of the magnetization are attributed to mullite. To explain the magnetic properties of this material, a model of the formation of ferrons with electron hoppings between sublattices from ferrous iron impurity ions with the absorption of optical magnons was proposed.

The space modulated $BiFeO_3$ structure can be suppressed differently, e.g., by applying a strong magnetic field, substituting rare-earth ions for Bi, and production of thin films [21–23]. Another way to suppress the modulation is to create multiphase compounds. Recently, a new direction has appeared in condensed matter physics, which studies multiphase systems consisting of compounds with different crystallographic structures and types of magnetic ordering. For example, the $Bi_2Fe_4O_9$–$BiFeO_3$ composite was synthesized using a sonochemical route and contained 90–94% of antiferromagnetic $BiFeO_3$ and 10–6% of mullite $Bi_2Fe_4O_9$. Average particle sizes of 13–57 nm for $BiFeO_3$ and 112–119 nm for $Bi_2Fe_4O_9$ for each percentage, respectively, were reported [24,25]. The coexistence of several magnetic states at helium temperatures, including a ferromagnetically ordered core, an antiferromagnetic shell, a super spin glass at the interface, and an asymmetric hysteresis loop, has been established.

The aim of this work was to define the effect of the synthesis technique, concentration of the $Bi_2Fe_4O_9/BiFeO_3$ phases, and particle size on the structural and magnetic properties of the material.

2. Material and methods

The investigated compound was synthesized by the solid-state reaction according to the scheme.

$2.5Bi_2O_3 + 2.5Fe_2O_3 \rightarrow 2Bi_2Fe_4O_{9-x}/BiFeO_{3-y}$.

The initial materials for the synthesis were oxides Bi_2O_3 and Fe_2O_3 of special purity grade (99.9%). The initial oxide mixture was thoroughly ground to a homogeneous state and tableted. The tablets were placed in a furnace and held at a temperature from 973 to 1173 K; the holding time varied from 8 to 24 h. The tablets were annealed in several stages with intermediate grinding.

The powder diffraction data on the $Bi_2Fe_4O_9/BiFeO_3$ composite for the Rietveld analysis were collected at room temperature using a Bruker D8 ADVANCE powder diffractometer (the analytical equipment of the Krasnoyarsk Regional Center for Collective Use, Krasnoyarsk Scientific Center, Siberian Branch of the Russian Academy of Sciences) equipped with a VANTEC linear detector (CuKα radiation). The 2θ step size was 0.016° and the counting time was 2 s per step. These structures were taken as a starting model for the Rietveld refinement performed using the TOPAS 4.2 software [26].

The morphology and qualitative and semi-quantitative elemental composition studies, as well as energy-dispersive elemental analysis of the synthesized composite were carried out on Hitachi SU3500 and TM 4000 scanning electron microscopes. Scanning electron microscope Hitachi SU3500 has a magnification of 3–300000, resolution up to 3 nm, depth of field 0.5 mm. Accelerating voltage 5–30 kV. The scanning electron microscope TM 4000 has a magnification of 10–100000, a depth of field of 0.5 mm, and a maximum displacement step of 65 nm. Accelerating voltage 15 kV. The EDS microanalysis system for the Hitachi TM 4000 electron microscope has an energy resolution of 137 eV (Mn Ka). Elemental mapping in the wave and energy dispersion modes adequately reflects the distribution of elements in the sample. The crystal structures of the composite components were determined in the backscattered electron mode. The tilt angle was 70°. The scanning of different sample microregions yielded identical results.

The infra-red (IR) spectroscopy study of the $Bi_2Fe_4O_9/BiFeO_3$ composite was carried out on an FSM 2202 IR Fourier spectrometer with a spectral resolution of 0.5 cm^{-1} at temperatures of 80–500 K and frequencies of 400–7000 cm^{-1} on the sample in the form of tablets with a diameter of 13 mm in a KBr matrix.

The thermal expansion coefficient β was determined from the change in linear sizes (dL/L) of the sample, which were found by measuring the electrical resistance of strain gauges located on the sample: $\beta = dR/dT \cdot 1/R$, where R is the electrical resistance of a load cell. Resistance was measured by Agilent 34420 A NanoVolt/Micro-Ohm Meter 7½ digits resolution.

The ultrasound damping coefficient in $Bi_2Fe_4O_9/BiFeO_3$ was determined on tablets with a thickness of 0.4 cm with two piezoelectric sensors glued to the tablet planes; one of them was a generator and the other, a receiver of ultrasonic waves. The ultrasound pulse duration time was $\tau = 10^{-7}$ s at a pulse repetition rate of 5 MHz. The formula for the calculation was

$$\alpha = \frac{\ln\left(\frac{U_1}{U_2}\right)}{d},$$

where U_1 and U_2 are the voltage amplitudes detected by the oscillation generator and receiver and d is the tablet thickness.

The magnetostriction was determined from the change in the linear sizes (dL/L) of the sample in a magnetic field by measuring the electrical resistance using Agilent 34420 A NanoVolt/Micro-Ohm Meter 7½ digits resolution. The sample with an attached strain gauge was placed between the electromagnet poles. The magnetostriction constant of the sample was calculated as

$$\lambda = \frac{R_H - R_0}{R_0},$$

where R_H and R_0 are the load cell resistances measured in nonzero and zero magnetic fields, respectively.

The magnetic properties of the composite were examined on a PPMS-9 Physical Property Measurement System at temperatures of up to 300 K in magnetic fields of $-6\ T < H < 6\ T$ in two modes. In the zero-field cooling (ZFC) mode, the sample was cooled down to the liquid helium temperature without field; after that, the magnetic field $H = 1000$ Oe was switched on and the magnetic moment was measured upon heating the sample. In the field cooling (FC) mode, the sample was cooled in a magnetic field of 1000 Oe and then its magnetic moment was measured in a magnetic field of 1000 Oe.

3. Results and discussion

3.1. X-ray diffraction and morphology

According to the X-ray diffraction data, the $Bi_2Fe_4O_9/BiFeO_3$ composite consists of $Bi_2Fe_4O_9$ (67%) and $BiFeO_3$ (33%) (Fig. 1). Atomic coordinates were fixed. The refinement was stable and yielded low R factors (see Table 1).

Fig. 2a shows a microphotograph of the $Bi_2Fe_4O_9/BiFeO_3$ composite surface. It can be seen that $Bi_2Fe_4O_9$ crystallites are tightly distributed and surrounded by smaller $BiFeO_3$ particles. The microphotograph shows the presence of pores in the sample. Fig. 2b shows the phase map obtained on the surface polished with argon.

Fig. 3 presents the $Bi_2Fe_4O_9$ grain distribution. The average size of $Bi_2Fe_4O_9$ crystallites is 1.5–4.0 μm. The $BiFeO_3$ grain size is smaller than the instrument resolution (100 nm).

The electron backscatter diffraction study (Fig. 4) established two orthorhombic crystalline phases $Bi_2Fe_4O_9$ and $BiFeO_3$ (sp. gr. *Pbam* and *R3c*), which is consistent with the X-ray diffraction data.

Fig. 5 shows the total energy spectrum of the $Bi_2Fe_4O_9/BiFeO_3$ composite. Its elemental composition corresponds to the chemical formulae of the components and agrees with the X-ray diffraction

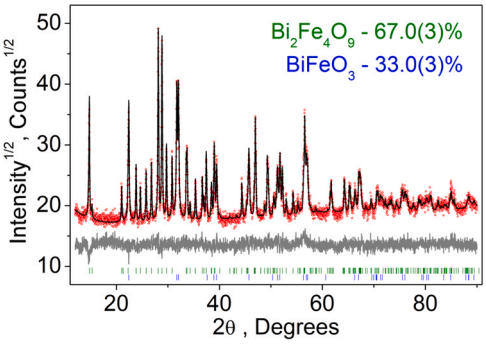

Fig. 1. Difference XRD pattern of the $Bi_2Fe_4O_9/BiFeO_3$ composite. The upper curve shows the experimental XRD pattern; the middle curve, the theoretical XRD pattern; and the lower curve, the difference between the theoretical and experimental XRD patterns.

Table 1
Structural parameters of the $Bi_2Fe_4O_9/BiFeO_3$ composite.

Phase	Weight, %	Space Group	Cell Parameters (Å), Cell Volume (Å3)	R_B	R_{wp}, R_p, χ^2
$Bi_2Fe_4O_9$	67.0 (3)	*Pbam*	a = 7.9793(4), b = 8.4468(4), c = 6.0072(3), V = 404.89(3)	1.35	5.93, 4.65, 1.23
$BiFeO_3$	33.0 (3)	*R3c*	a = 5.5821(3), c = 13.8737(9), V = 374.39(5)	1.81	

data. The calculated atomic and mass fractions (per cent) in the phase components $Bi_2Fe_4O_9$ and $BiFeO_3$ in the composite are in good agreement with the experiment (Table 2).

3.2. IR spectroscopy study

The IR spectrum of the $Bi_2Fe_4O_9/BiFeO_3$ composite represents a set of lines corresponding to its components. The group-theoretical analysis revealed 14 IR active modes B2u [27] (see Table 3) and 42 Raman active modes (12Ag +12B1g+ 9B2g + 9B3g) [12] for $Bi_2Fe_4O_9$. According to the group theory, there are 18 optical phonon modes in $BiFeO_3$: 4A1 + 5A2 + 9E are active. Phonon modes A1 and E are active both in Raman and IR spectroscopy (Table 4) and A2 is only active in the Raman mode [28].

Fig. 6 presents the IR spectrum of the $Bi_2Fe_4O_9/BiFeO_3$ composite at temperatures from 80 to 480 K.

The absorption band in the frequency range of $w = 530–628\ cm^{-1}$ is described by two Lorentz curves. The mode at a frequency of $w = 535\ cm^{-1}$ slightly softens with temperature and vanishes at $T = 280$ K in the temperature region of the maximum magnetic susceptibility and maximum thermal expansion coefficient (inset in Fig. 7b). Vibrations at a frequency of $602\ cm^{-1}$ are attributed to

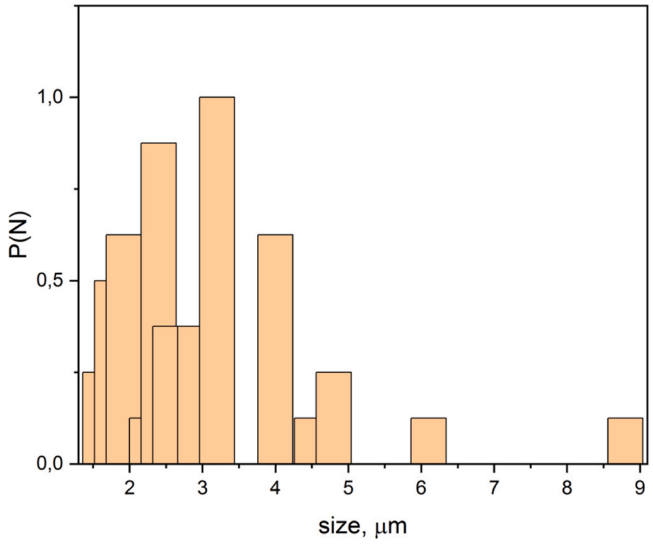

Fig. 3. The grain size distribution functions of the $Bi_2Fe_4O_9/BiFeO_3$ composite.

bending vibrations of the O–Fe–O and Fe–O–Fe bonds in the FeO_4 tetrahedral pairs of the Fe_2O_7 dimer of the $Bi_2Fe_4O_9$ ceramics [29]. The mode $w = 602\ cm^{-1}$ is softened by $3\ cm^{-1}$ at 200 K (Fig. 7a), where the magnetostriction constant attains its maximum.

The next mode in the IR spectrum of the $Bi_2Fe_4O_9/BiFeO_3$ composite at a frequency of $w = 637\ cm^{-1}$ at room temperature corresponds to stretching vibrations of the Fe–O bonds in FeO_4 tetrahedra of $Bi_2Fe_4O_9$ [29] and stretching vibrations of Fe^{3+} in FeO_6 octahedra of $BiFeO_3$ [30]. The mode $w = 637\ cm^{-1}$ is softened in frequency by 2% at 240 K and the derivative dw/dT of this mode has the maximum absolute value (inset in Fig. 6). The dw/dT maxima of these modes are observed also in the range of 320–360 K.

The symmetrical mode $w = 815\ cm^{-1}$ is softened by $5\ cm^{-1}$ (Fig. 7c) in the region of the $Bi_2Fe_4O_9$ magnetic phase transition and is consistent with vibration frequencies of $w = 812\ cm^{-1}$ for $BiFeO_3$ and $w = 815\ cm^{-1}$ for $Bi_2Fe_4O_9$. In the $BiFeO_3$ ceramics, the mode softening at a frequency of $w = 812\ cm^{-1}$ is caused by the reorientation of ions [31]. In $Bi_2Fe_4O_9$, the mode $w = 815\ cm^{-1}$ corresponds to stretching vibration of the Fe–O bonds in FeO_4 tetrahedra [29].

According to the lattice dynamical calculation (LDC), the absorption peak at a frequency of $535\ cm^{-1}$ corresponds to Raman mode B1g at a frequency of $545\ cm^{-1}$ and is caused by a combined mode consisting of a magnetic vibration mode and a vibrational mode of FeO_4 tetrahedra [12]. Vanishing of the magnetic vibration mode in the region of the magnetic phase transition leads to an increase in the intensity of the FeO_4 vibrational mode by 5%. The mullite structure contains tetrahedra of two types, which belong to the B2u vibrational symmetry and are related to the Fe–O stretching

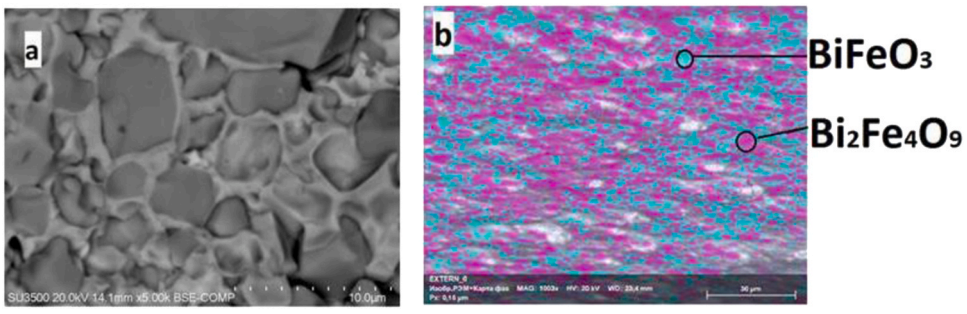

Fig. 2. SEM image of the $Bi_2Fe_4O_9/BiFeO_3$ composite: a) surface microphotography, b) phase map.

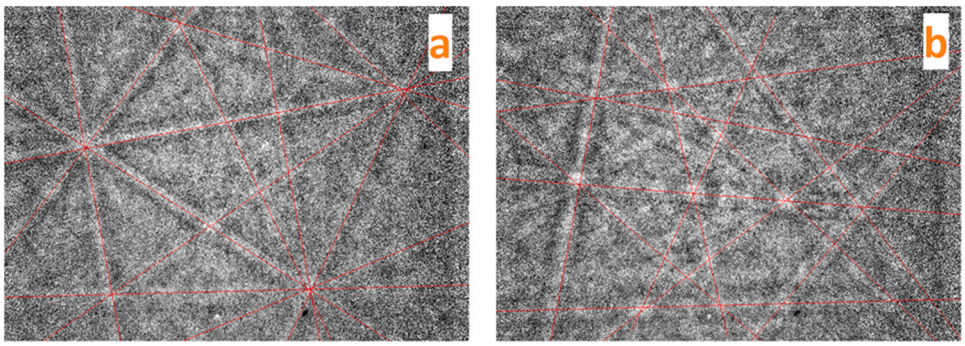

Fig. 4. The diffraction of the $Bi_2Fe_4O_9/BiFeO_3$ composite: a) $Bi_2Fe_4O_9$, b) $BiFeO_3$.

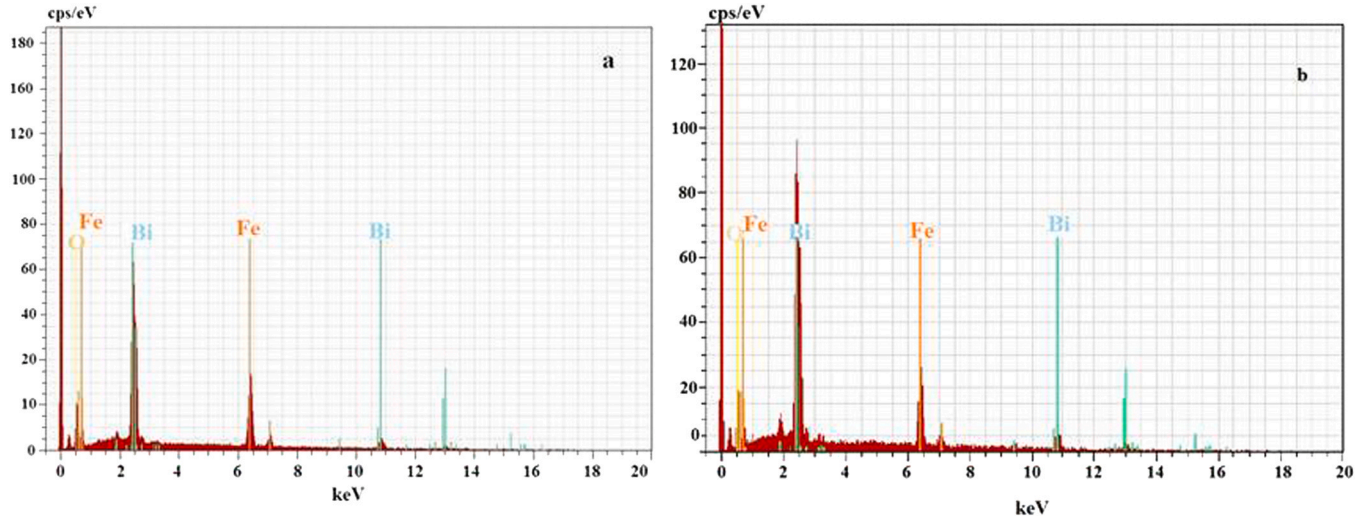

Fig. 5. EDS of the $Bi_2Fe_4O_9/BiFeO_3$ composite. (a) EDS of $Bi_2Fe_4O_9$ phase. (b) EDS of $BiFeO_3$ phase.

Table 2
Atomic and mass ratio of elements of the $Bi_2Fe_4O_9$ and $BiFeO_3$.

element	$Bi_2Fe_4O_9$				$BiFeO_3$			
	Theoretical calculations		Experimental data		Theoretical calculations		Experimental data	
	Atomic %	Mass %	Atomic %	Mass %	Atomic %	Mass %	Atomic %	Mass %
oxygen	60	18.32	50.76	14.11	60	15.33	50.10	13.21
iron	26,7	28.5	34.90	33.86	20	17.9	24.34	19.95
bismuth	13,3	53.18	14.33	52.03	20	66.77	25.56	66.84

Table 3
Calculated and experimental data of active Raman and IR modes in $Bi_2Fe_4O_9$.

Raman mode	Raman LDC $Bi_2Fe_4O_9$, $см^{-1}$[12]	Mode IR	IR LDC $Bi_2Fe_4O_9$, $см^{-1}$[27].	IR modes of $Bi_2Fe_4O_9/BiFeO_3$ at T = 280 K, cm^{-1} in this article	Atomic motions[32]
B1g	545	B2u		535	Fe –M– Fe bend (FeO4)
B1g	606	B2u		602	Fe–O–Fe bend (FeO4)
B1g	628	B2u	639	638	Fe–O stretch (FeO4)
B1g	813	B2u	789	814	Fe –O stretch (FeO4)

modes at frequencies of 635 and 815 cm^{-1}. The exchange coupling between iron ions is carried out through oxygen and the disappearance of the exchange energy in the region of the magnetic phase transition leads to a decrease in the effective modulus of elasticity and, consequently, in the oscillation frequency of these modes. The mode $w = 815\ cm^{-1}$ is softened at 440 K.

3.3. Thermal expansion coefficient

Fig. 8 shows the temperature dependence of the thermal expansion coefficient of the $Bi_2Fe_4O_9/BiFeO_3$ composite heated in zero field and cooled and heated in a magnetic field of $H = 12$ kOe. The $\beta(T)$ change under the magnetic field is explained by the

Table 4
IR active modes in $BiFeO_3$ using notations [33].

Mode	Calculated[33],см$^{-1}$	Modes observed in[30] at T = 303 K, cm^{-1}	Modes observed in[31] at T = 300 K, cm^{-1}	Modes of $Bi_2Fe_4O_9/BiFeO_3$ at T = 280 K, cm^{-1} in this article	Atomic motions [30]
E(TO5)	274	307			Fe^{3+} internal vibration in FeO_6 octahedra
A1(TO3)	318	331			Fe^{3+} internal vibration in FeO_6 octahedra
E(TO6)	335	351			Fe^{3+} internal vibration in FeO_6 octahedra
E(TO7)	378	391			vibration Fe^{3+} cations in FeO_6 octahedra
E(TO8)	409	437			Fe-O bend
E(TO9)	509	551	545(A1 (TO))	526	Fe-O stretch
		638		638	local lattice distortion of FeO_6 octahedra
			814		combining

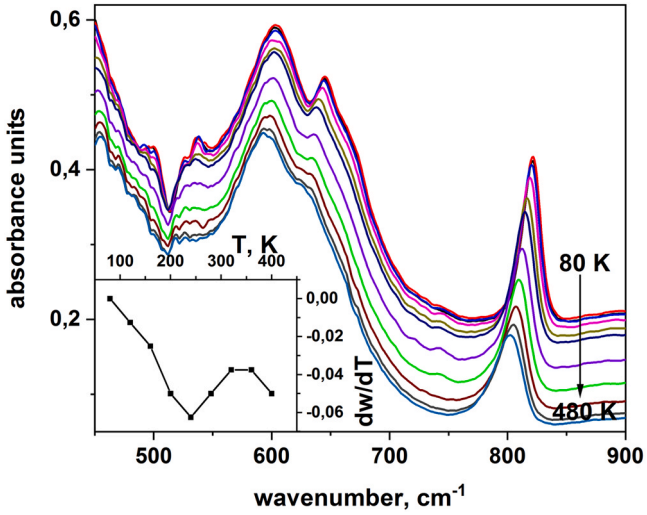

Fig. 6. Infrared spectra of the $Bi_2Fe_4O_9/BiFeO_3$ composite at several temperatures. The inset shows the derivative d*w*/dT mode of the mode w= 637 см$^{-1}$.

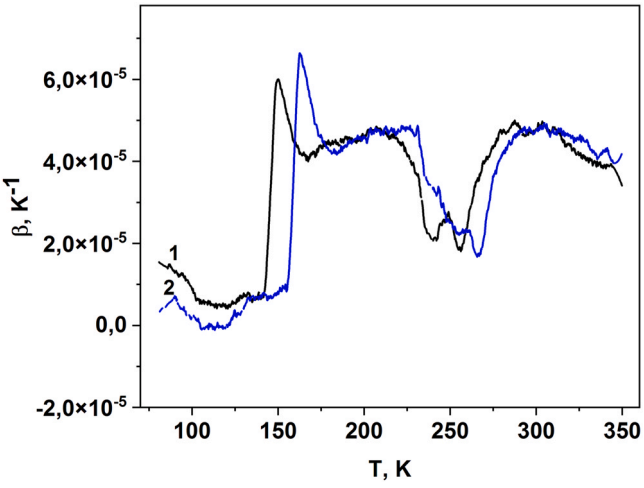

Fig. 8. The temperature dependence of thermal expansion coefficient of $Bi_2Fe_4O_9/BiFeO_3$ composite, curve 1 corresponds to heating the sample in the magnetic field H= 0 kOe, 2- H= 12 kOe.

magnetostriction and domens structure that disappears in magnetic field. The β(T) maximum at 150 K in zero magnetic field shifts to a temperature of 163 K in a magnetic field of H = 12 kOe. In the temperature range of 240–270 K, the expansion of the sample caused by bismuth ferrite is partially compensated by the compression of mullite crystallites. Ferromagnetic drops are formed in the vicinity of the magnetic phase transition in $Bi_2Fe_4O_9$, which lead to lattice compression. According to the literature data, the $Bi_2Fe_4O_9$ Néel temperature lies in the region from 240 K [12,34] to 265 K [13,35]. This temperature interval is consistent with the disappearance of the phonon mode w = 535 cm^{-1}. The β(T) jump around 150 K correlates with the impedance jump in the $BiFeO_3$ films [5]. Below 150 K, a magnetization hysteresis is arises, where the remanent magnetization also sharply drops by an order of magnitude (Fig. 10).

A broad β(T) maximum at room temperature correlates with the maximum magnetization of the film BiFeO3 in the temperature range 280–350 K (insert of Fig. 11).

3.4. Magnetic properties

The $Bi_2Fe_4O_9/BiFeO_3$ composite exhibits the properties of an antiferromagnet. The ZFC and FC temperature dependences of its magnetic susceptibility are shown in Fig. 9. The magnetic susceptibility increases smoothly upon heating above 40 K and, at T = 250 K, has a kink-like singularity, which is observed in a mullite single crystal. Above a transition temperature of T = 250 K, the magnetic susceptibility has a broad maximum.

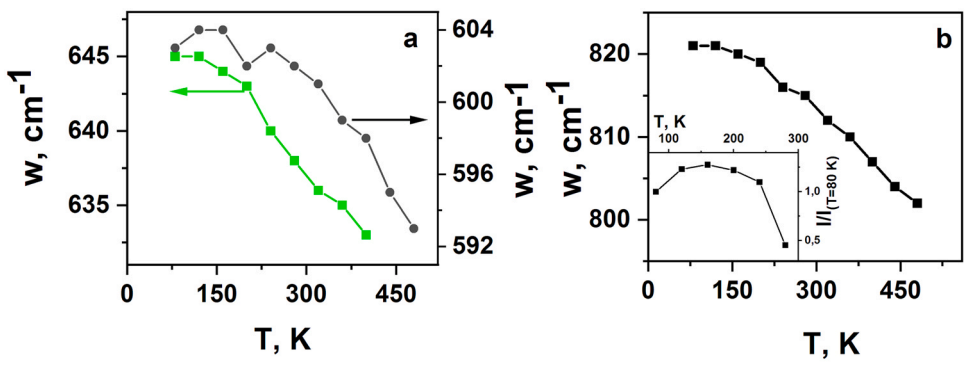

Fig. 7. The temperature dependence of phonon frequencies of $Bi_2Fe_4O_9/BiFeO_3$ composite. The inset shows the temperature dependence of the relative intensity of the mode with frequency w= 535 см$^{-1}$.

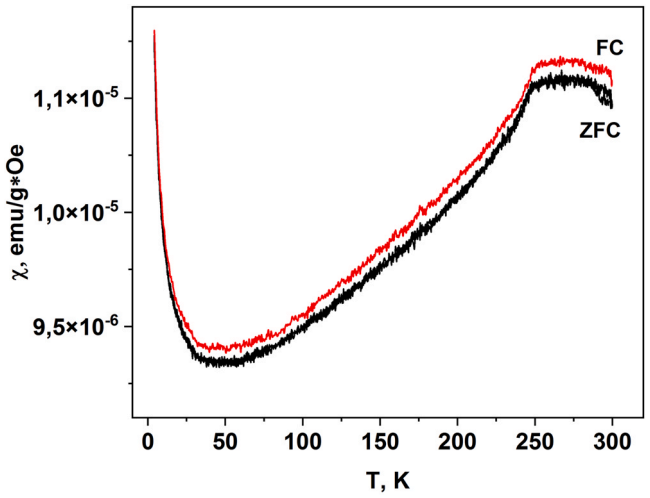

Fig. 9. The temperature dependence of magnetic susceptibility of $Bi_2Fe_4O_9/BiFeO_3$ composite.

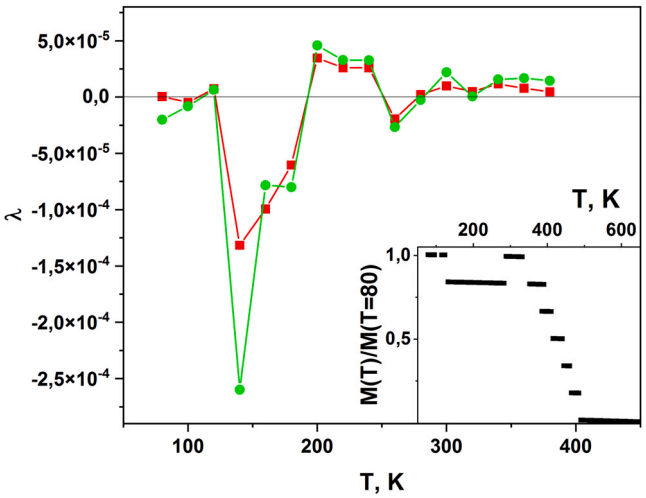

Fig. 11. The temperature dependence of the magnetostriction coefficient of $Bi_2Fe_4O_9/BiFeO_3$ composite in the magnetic fields H= 6 and 12 kOe. The square symbols correspond to the magnetic field of 6 kOe, the round ones to 12 kOe. The inset shows the temperature dependence of magnetization of the $BiFeO_3$ film in the magnetic field H= 8600 Oe.

The field dependence of the magnetization has a hysteresis (Fig. 10a), where the magnetization does not saturate. The temperature dependence of the coercivity H_c (inset in Fig. 10b) has the maximum at $T = 50$ K and vanishes at 150 K. The remanent magnetization decreases upon heating; at $T = 4.2$ K the remanent magnetization is 0.0015 emu/g and, at $T = 150$ K, it sharply decreases by a factor of 3.5 (Fig. 10b).

The $BiFeO_3$ bulk compound has a space modulated antiferromagnetic structure with a cycloid period of $\lambda c \approx 62$ nm [36] and, below 160 K, exhibits the spin-glass behavior. The field dependence of the magnetization has hysteretic at temperatures of 5 and 300 K, where the magnetization saturates [30,37]. The magnetization of $BiFeO_3$ is low and increases linearly with an increase in the magnetic field, which is typical of antiferromagnets [38–40]. In the case of $Bi_2Fe_4O_9$, the magnetic hysteresis depends strongly from the crystallite size and vanishes above its critical value of 1 μm. The average size of mullite nanocrystallites in our sample is 2–4 μm; therefore, mullite does not contribute to the magnetic hysteresis of the $Bi_2Fe_4O_9/BiFeO_3$ composite. Hence, the magnetic hysteresis is related to bismuth ferrite $BiFeO_3$ nanoparticles.

In polycrystalline bismuth ferrite $BiFeO_3$, the uncompensated magnetic moment is formed if the crystallite size is comparable to the cycloid period (62 nm). Study on an electron microscope with a resolution of 100 nm did not allow us to determine the $BiFeO_3$ crystallite size in the investigated composite; therefore, we assume that the crystallite size is about the cycloid wavelength.

In thin films of $BiFeO_3$ with a thickness of 565 nm, the hysteresis M(H) with residual magnetization $M_r = 0.9$ emu/g= 0.04 μ_B/f.u. and coercive field 50 Oe was found [41]. The canted angle of the sublattices is $\vartheta = M_r/M = 0.004$ and is in the range of angles 0.001–0.01 formed by antisymmetric exchange $\vartheta = D/(2J + 3K)$, where D is the Dzyaloshinsky-Moriya parameter, K is the anisotropy constant, J-exchange [42]. The remanent magnetization is two orders of magnitude smaller and $M_r = 0.006$ emu/g in nanocrystals with a crystallite size of 25–30 nm [43,44]. The formation of hysteresis with a weak residual magnetic moment is attributed to the non-compensation of surface spins. The difference of the spins number in the sublattices on the crystallite surface is the source of the magnetic moment in the antiferromagnet. A crystallite in the kind of a cube with a side of 60 nm has a magnetization per formula unit $M \sim 0.8\ 10^{-4}$ μ_B/f.u = 0.0015 emu/g, if there is an uncompensated spin on each face of the cube with $\mu = 5\ \mu_B$. The crystallites in the composite have a G-type AFM structure, which changes at 140 K as a result of a structural transition. The magnetization of the polycrystalline $BiFeO_3$ film decreases jumpily by 15% in a magnetic field of 0.86 T at T = 132 K (Inset Fig. 11). The frequency of the E-type phonon mode in $BiFeO_3$ nanotubes sharply increases from 83 cm^{-1} to 97 cm^{-1} above 140 K [5]. Similar behavior was found in ceramics and single crystals. The phonon mode is associated with the vibration of the Bi-O bond. In bulk samples, the frequency decreases to 75 cm^{-1} and the

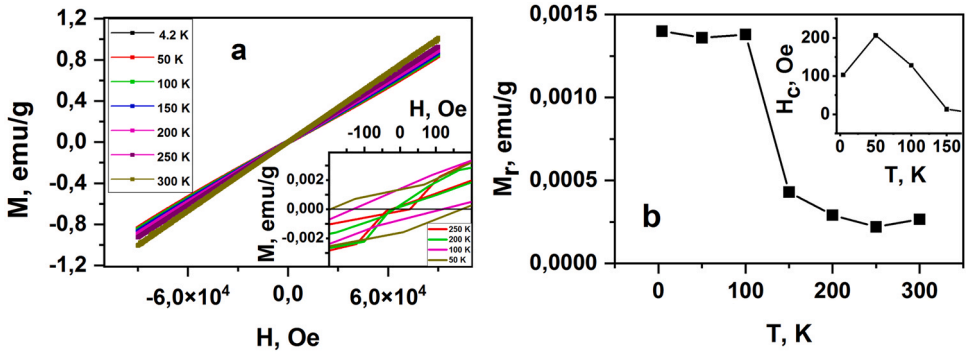

Fig. 10. a) The field dependence of magnetization of the $Bi_2Fe_4O_9/BiFeO_3$ composite. In the inset the field dependence of magnetization in the magnetic field from – 200–200 Oe at temperatures 50, 100, 200 and 250 K. b) The temperature dependence of the remanent magnetization of the $Bi_2Fe_4O_9/BiFeO_3$ composite. The inset shows the temperature dependence of the coercive field.

temperatures of the maxima ω(T) are shifted to the region of low temperatures. The magnon modes show small sharp peaks around 130 K and 225 K, 130 K and 200 K. The intensities of these modes also have anomalies at the same temperatures [45,46]. These anomalies are explained by the reorientation of the spin and the change in the elastic characteristics. As a result, the indirect exchange interaction between Fe^{3+} ions in $BiFeO_3$ changes, since its value depends from the Fe-O-Fe bond angle and the Fe-O bond length. Spin-reorientation transition associated with a change of magnetic anisotropy upon heating. The change of frequency is attributed to the displacement of the oxygen ion, which will lead to a change in the antisymmetric exchange. So, the parameter $D \sim [r_1, r_2] \sim \lambda \cdot U_i$, where r_1, r_2 are the bond vectors of the oxygen ion with the nearest iron ions Fe_1-O and Fe_2-O, U_i is the relative displacement of the oxygen ion, λ is the spin-orbit interaction constant. In the region of the structural transition, there is degeneracy in the oxygen displacement, for example ± U, and, accordingly, in the sign of the antisymmetric exchange. In $BiFeO_3$ nanocrystals above 140 K, an incommensurable magnetic structure (probably spiral) with threefold degeneracy in direction is formed, which can be lifted by a magnetic field. This effect will manifest itself in magnetostriction.

3.5. Magnetostriction

The change of the magnetic structure upon heating in a magnetic field as a result of the magnetoelastic interaction can be detected by measuring the deformation of the samples. There are no data about magnetostriction of $Bi_2Fe_4O_9$ and $BiFeO_3$ compounds. Fig. 11 shows the temperature dependence of the magnetostriction constant of the $Bi_2Fe_4O_9/BiFeO_3$ composite measured in magnetic fields of $H = 6$ and 12 kOe. It can be seen that the magnetostriction constant depends on the magnetic field. The temperatures of the maximum magnetostriction constant and the ultrasound damping coefficient (Fig. 12) are corresponds with a temperature of $T = 140$ K of the structural surface phase transition in $BiFeO_3$. The $BiFeO_3$ lattice constant increases sharply above 140 K [5], which is in qualitative agreement with our $\beta(T)$ data. In the region of the transition, the magnetostriction constant grows linearly with an increase in the magnetic field. The temperature shift of the maximum of the thermal expansion coefficient β(T) towards higher temperatures in a magnetic field and an increase of the intensity of ultrasound damping indicate to the relationship between magnetic and structural characteristics.

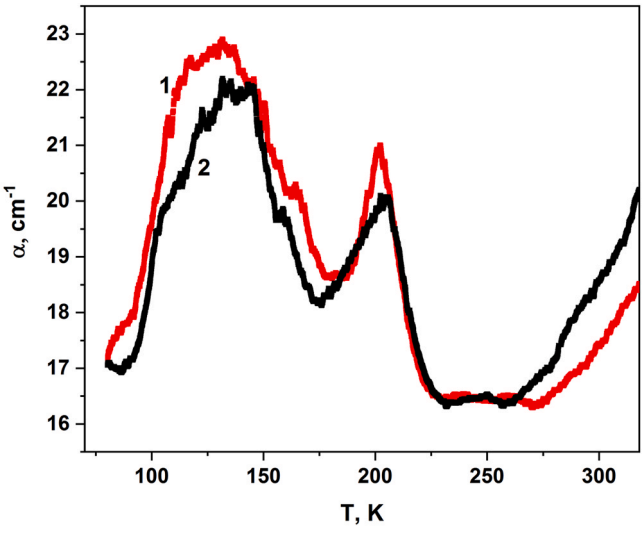

Fig. 12. The temperature dependence of the sound damping coefficient of the $Bi_2Fe_4O_9/BiFeO_3$ composite. The curve 1 corresponds to the sound damping coefficient in the magnetic field 12 kOe, while curve 2 corresponds to the same without any field.

At 200 K, the magnetostriction constant changes its sign, which is associated with a change in the magnetoelastic constants. The temperature of a spin reorientation transition in $BiFeO_3$ correlates with the temperature of softening of Raman mode E3 at a frequency of 268 cm^{-1} at T = 200 K [28]. The phonon mode frequencies are determined by the modulus of elasticity; therefore, the shift of Raman scattering lines is indicative of the change in the magnetoelastic constant. The IR spectroscopy study of the spin−phonon interaction in the $BiFeO_3$ compound revealed two new phonon modes, E and A1, at $T = 213$ K, which are attributed to Fe^{3+} vibrations in the FeO_6 octahedron [30]. As the temperature decreases, the intensity of these modes grows due to the lattice compression. The appearance of additional modes is caused by the reorientation of Fe^{3+} spins [30] as a results of the spin−phonon interaction, which is confirmed also by the g-factor anomaly at $T = 201$ K found during the electron spin resonance (ESR) measurements [5].

In the range of the magnetic phase transition in mullite, the magnetostriction constant changes its sign; the thermal expansion coefficient is minimum at 255 K and shifts in a magnetic field to 266 K. Mullite, similar to bismuth ferrite, is characterized by the magnetoelastic interaction. At room temperature and above it, the positive magnetostriction constant is related to bismuth ferrite.

There are two main mechanisms of magnetostriction: single-ion with an orbital magnetic moment of the magnetic ion [47]. In a magnetic field, the rotation of the orbital momentum changes the electrostatic field of the surrounding ions; as a result, the crystal lattice undergoes anisotropic deformations. Exchange magnetostriction (λ) arise at the exchange interaction between magnetic ions changes and is associated with spin correlators. Exchange magnetostriction [48]:

$$\lambda \sim (B_{[100]} - B_{[111]})\langle \vec{S}(0)\vec{S}(h)\rangle/(C_{11} - C_{14}) \quad (1)$$

where B is the exchange magnetoelastic constant, C_{11}, C_{14} are the elastic modules for a cubic crystal, $\langle \vec{S}(0)\vec{S}(h)\rangle$ is the spin-spin correlation function between nearest neighbors. A slight uniaxial pressure (70 bar) in a single crystal of bismuth ferrite doped with 2% Nd rotates the easy plane of magnetic anisotropy by 60° [49] and creates deformations of 10^{-5}–10^{-4}, which are 2–3 orders of magnitude smaller than the deformations during the structural transition [50,51]. The plane of a magnetic cycloid can rotate due to temperature-induced deformation created by surface energy in nanocrystallites. The change of sign of the magnetostriction constants occurs when the magnitude of the magnetoelastic constants changes in the vicinity of 200 K. The correlator $\langle \vec{S}(0)\vec{S}(h)\rangle$ between the spins of iron ions in $BiFeO_3$ is negative. The magnetostriction constant is positive when the relation $B_{[111]} > B_{[100]}$ is satisfied.

Thus, at 140 K the magnetic structure of $BiFeO_3$ changes from the Neel AFM to the incommensurate one. Magnetic domains with triple degeneracy among the direction of the incommensurability vector in the transition region are created. This degeneracy is removed by a magnetic field, which leads to lattice compression. Ferromagnetic drops (ferrons) are formed in mullite in the region of magnetic phase transition temperature [20]. The appearance of the ferromagnetic component of the exchange causes compression of the drop. In a magnetic field, the volume of the ferron grows, and the sample is compressed. As a result of the competition between the two factors in mullite and bismuth ferrite, the magnetostriction constant becomes negative in the range 250–260 K.

3.6. Acoustic properties

The temperature dependences of ultrasound damping coefficient α in zero magnetic field and in a field of $H = 12$ kOe are presented in Fig. 12. It can be seen that the $\alpha(T)$ curve has several anomalies, the temperatures of which depend on the magnetic field. The low-

temperature α anomaly is caused by the structural and magnetic transition in $BiFeO_3$ at $T = 140$ K. The increase of ultrasound damping in magnetic field is caused by the magnetoelastic interaction. A strong influence of the magnetic field on the ultrasound damping was found in the region of the orientational magnetic transition at 200 K, where the ultrasound damping intensity increases by a factor of 1.5, as a result of softening of polar Raman mode E3 at a frequency of 268 cm^{-1}. An increase of ultrasonic damping in a magnetic field is due to the magnetoelectric interaction. An increase in the ultrasound damping coefficient above 270 K and a broad maximum of the thermal expansion coefficient in the room temperature region are caused by softening of the Fe–O stretch satellite mode of the tetrahedron in mullite at a frequency of 635 cm^{-1}.

4. Conclusions

It was shown that the synthesized $Bi_2Fe_4O_9/BiFeO_3$ composite differs from previously known in the percentage of phases in the sample, synthesis technique used, and particle size. An increase of the mullite concentration and the average particle size leads to a change of the magnetic properties of the composite. Study of the morphological properties of the $Bi_2Fe_4O_9/BiFeO_3$ composite demonstrated that $Bi_2Fe_4O_9$ crystallites have an average size of 1.5–4.0 μm and are surrounded by $BiFeO_3$ crystallites smaller than 100 nm in size.

Using IR spectroscopy, vibrational modes of tetrahedra and octahedra and their softening temperatures were established. The relationship between the phonon modes and magnetic order of the composite was determined. A kink in the temperature dependence of the magnetic susceptibility of the composite at the temperature of the magnetic phase transition in mullite was found, which is not observed in single-phase mullite. The magnetic hysteresis induced by bismuth ferrite nanoparticles and the critical temperature of disappearance of the coercivity and remanent magnetization, which is a property of the composite, was established. A change in the sign of the magnetostriction constant and, consequently, of the magnetoelastic constants was found with a change in temperature near the temperature of the spin-reorientation transition in $BiFeO_3$ crystallites and at the Néel temperature in mullite. An increase of the magnetostriction constant and ultrasound damping on a magnetic field near the temperature of the surface phase transition and at the temperature of the spin reorientation transition in $BiFeO_3$ in the composite was observed. The contributions of each phase to the structural and magnetic transitions in the $Bi_2Fe_4O_9/BiFeO_3$ composite were determined.

CRediT authorship contribution statement

L.V. Udod- Investigation, Visualization, Writing – original draft. **S.S. Aplesnin**: Supervision, Conceptualization, Methodology, Writing – review & editing. **M.N. Sitnikov:** Investigation. **M.N. Molokeev:** Investigation. **O.B. Romanova**: Validation, Visualization. **E.V. Eremin**: Investigation. **A.V. Shabanov**: Investigation. **A.M. Kharkov:** Investigation.

Data Availability

No data was used for the research described in the article.

Declaration of Competing Interest

The authors declare that they have no known competing financial interests or personal relationships that could have appeared to influence the work reported in this paper.

Appendix A. Supporting information

Supplementary data associated with this article can be found in the online version at doi:10.1016/j.jallcom.2023.170445.

References

[1] J. Wang, J. Neaton, H. Zheng, V. Nagarajan, S. Ogale, B. Liu, D. Viehland, V. Vaithyanathan, D. Schlom, U. Waghmare, Epitaxial $BiFeO_3$ mutliferroic thin film heterostructures, Science 299 (2003) 1719–1722, https://doi.org/10.1126/science.1080615

[2] W. Erenstein, N. Mathur, J. Scott, Multiferroic and magnetoelectric materials, Nature 442 (2006) 759–765, https://doi.org/10.1038/nature05023

[3] A.K. Zvezdin, A.P. Pyatakov, Phase transitions and giant magnetoelectric effect in multiferroics, Phys. Usp. 174 (2004) 416–421, https://doi.org/10.3367/UFNr.0174.200404n.0465

[4] P. Fischer, M. Polomska, I. Sosnowska, M. Szymanski, Temperature dependence of the crystal and magnetic structures of $BiFeO_3$, J. Phys. C: Solid St. Phys. 13 (1980) 1931-40.

[5] R. Jarrier, X. Marti, J. Herrero-Albillos, P. Ferrer, R. Haumont, P. Gemeiner, G. Geneste, P. Berthet, T. Sch¨ulli, P. Cevc, R. Blinc, S.Wong Stanislaus, Park Tae-Jin, M. Alexe, M.A. Carpenter, J.F. Scott, G. Catalan, B. Dkhil, Surface phase transitions in $BiFeO_3$ below room temperature, Phys. Rev. B 85 (2012) 184104, https://doi.org/10.1103/PhysRevB.85.184104

[6] A.G. Zhdanov, A.K. Zvezdin, A.P. Pyatakov, T.B. Oblique, D. Viehland, Effect of an electric field on magnetic transitions "incommensurate–commensurate phase" in a multiferroic of the BiFeO3 type, Solid St. Phys. 48 (2006) 83–89.

[7] F. Gao, C. Cai, Y. Wang, S. Dong, X.Y. Qiu, G.L. Yuan, Z.G. Liu, Preparation of La-doped $BiFeO_3$ thin films with Fe^{2+} ions on Si substrates, JAP 99 (2006) 094105, https://doi.org/10.1063/1.2195368

[8] G. Catalan, J.F. Scott, Physics and applications of bismuth ferrite, Adv. Mater. 21 (2009) 2463–2485, https://doi.org/10.1002/ADMA.200802849

[9] Y.A. Park, K.M. Song, K.D. Lee, C.J. Won, N. Hur, Effect of antiferromagnetic order on the dielectric properties of $Bi_2Fe_4O_9$, Appl. Phys. Lett. 96 (2010) 092506, https://doi.org/10.1063/1.3339880

[10] D.P. Dutta, C. Sudakar, P.S.V. Mocherla, B.P. Mandal, O.D. Jayakumar, A.K. Tyagi, Enhanced magnetic and ferroelectric properties in scandium doped nano $Bi_2Fe_4O_9$, Mater. Chem. Phys. 135 (2012) 998e1004, https://doi.org/10.1016/j.matchemphys.2012.06.005

[11] A. Kirsch, M.M. Murshed, F.J. Litterst, T.M. Gesing, Structural, spectroscopic, and thermoanalytic studies on $Bi_2Fe_4O_9$: tunable properties driven by nano-and poly-crystalline states, J. Phys. Chem. C. 123 (5) (2019) 3161–3171, https://doi.org/10.1021/ACS.JPCC.8B09698

[12] M.N. Iliev, A.P. Litvinchuk, V.G. Hadjiev, M.M. Gospodinov, V. Skumryev, E. Ressouche, Phonon and magnon scattering of antiferromagnetic $Bi_2Fe_4O_9$ (8), Phys. Rev. B 81 (2010) 024302, https://doi.org/10.1103/PhysRevB.81.024302

[13] N. Shamir, E. Gurewitz, H. Shaked, The magnetic structure of $Bi_2Fe_4O_9$ – analysis of neutron diffraction measurements, Acta Crystallogr. A 34 (1978) 662–666, https://doi.org/10.1107/S0567739478001412

[14] Z. Pchelkina, S. Streltsov, Ab initio investigation of the exchange interactions in Bi2Fe4O9: the Cairo pentagonal lattice compound, Phys. Rev. B 88 (2013) 054424, https://doi.org/10.1103/PhysRevB.88.054424

[15] J. Zhao, T. Liu, Y. Xu, Y. He, W. Chen, Synthesis and characterization of $Bi_2Fe_4O_9$ powders, Mater. Chem. Phys. 128 (2011) 388–391, https://doi.org/10.1016/j.matchemphys.2011.03.011

[16] G. Alvarez, J. Contreras, A. Conde-Gallardo, H. Montiel, R. Zamorano, Detection of para–antiferromagnetic transition in $Bi_2Fe_4O_9$ powders by means of microwave absorption measurements, J. Magn. Magn. Mater. 348 (2013) 17–21, https://doi.org/10.1016/j.jmmm.2013.08.014

[17] G.C. Papaefthymiou, A.J. Viescas, J.-M. Le Breton, H. Chiron, J. Juraszek, T.J. Park, S.S. Wong, Magnetic and Mössbauer characterization of the magnetic properties of single-crystalline sub-micron sized $Bi_2Fe_4O_9$ cubes, Curr. Appl. Phys. 15 (2015) 417–422, https://doi.org/10.1016/J.Cap.2014.11.008

[18] Z. Tian, S. Yuan, X. Wang, X. Zheng, S. Yin, C. Wang, L. Liu, Size effect on magnetic and ferroelectric properties in $Bi_2Fe_4O_9$ multiferroic ceramics, J. Appl. Phys. 106 (2009) 103912, https://doi.org/10.1063/1.3259392

[19] X. Wu, J. Miao, Y. Zhao, X. Meng, X. Xu, S. Wang, Y. Jiang, Novel multiferroic $Bi_2Fe_4O_9$ nanoparticles: the interesting optical, photocatalytic, and multiferroic properties, Optoelectron, Adv. Mater. -RAPID Commun. 7 (2013) 116–120.

[20] S.S. Aplesnin, L.V. Udod, M.N. Sitnikov, D.A. Velikanov, M.N. Molokeev, O.B. Romanova, A.V. Shabanov, Enhancement of ferromagnetism and ferroelectricity by oxygen vacancies in mullite $Bi_2Fe_4O_9$ in the $Bi_2(Sn_{0.7}Fe_{0.3})_2O_{7-x}$ matrix, JMMM 559 (2022) 169530, https://doi.org/10.1016/j.jmmm.2022.169530

[21] D. Lee, M.G. Kim, S. Ryu, H.M. Jang, S.G. Lee, Epitaxially grown La-modified $BiFeO_3$ magnetoferroelectric thin films, Appl. Phys. Lett. 86 (2005) 222903, https://doi.org/10.1063/1.1941474

[22] N. Wang, J. Cheng, A.P. Pyatakov, A.K. Zvezdin, J.F. Li, L.E. Cross, D. Viehland, Multiferroic properties of modified $BiFeO_3$–$PbTiO_3$-based ceramics: random-field induced release of latent magnetization and polarization, Phys. Rev. B 72 (2005) 104434, https://doi.org/10.1103/PhysRevB.72.104434

[23] J. Li, J. Wang, M. Wuttig, R. Ramesh, N. Wang, B. Ruette, A.P. Pyatakov, A.K. Zvezdin, D. Viehland, Dramatically enhanced polarization in (001), (101), and (111) $BiFeO_3$ thin films due to epitiaxial-induced transitions, Appl. Phys. Lett. 84 (2004) 5261, https://doi.org/10.1063/1.1764944

[24] T. Maity, S. Roy, Asymmetric ascending and descending loop shift exchange bias in $Bi_2Fe_4O_9$-$BiFeO_3$ nanocomposites, JMMM 494 (2020) 165783, https://doi.org/10.1016/j.jmmm.2019.165783
[25] T. Maity, S. Goswami, D. Bhattacharya, S. Roy, Superspin glass mediated giant spontaneous exchange bias in a nanocomposite of $BiFeO_3$-$Bi_2Fe_4O_9$, Phys. Rev. Lett. 110 (2013) 107201, https://doi.org/10.1103/PhysRevLett.110.107201
[26] A.X.S. Bruker, TOPAS V4: General profile and structure analysis software for powder diffraction data. – user's manual, Bruker AXS, Karlsr. Ger. (2008).
[27] M. Verseils, A.P. Litvinchuk, J.-B. Brubach, P. Roy, K. Beauvois, E. Ressouche, V. Skumryev, M. Gospodinov, V. Simonet, S. de Brion, Infrared phonon spectroscopy on the Cairo pentagonal antiferromagnet $Bi_2Fe_4O_9$: a study through the pressure induced structural transition, Phys. Rev. B 103 (2021) 174403, https://doi.org/10.1103/PhysRevB.103.174403
[28] Y. Yang, J.Y. Sun, K. Zhu, Y.L. Liu, J. Chen, X.R. Xing, Raman study of $BiFeO_3$ with different excitation wavelengths, Phys. B 404 (2009) 171–174, https://doi.org/10.1016/j.physb.2008.10.029
[29] H. Zhang, T. Tong, J. Chen, J. Cheng, Synthesis and visible light photocatalytic properties of $Bi_2Fe_4O_9$ particles via EDTA-assisted sol–gel route, J. Sol. -Gel Sci. Technol. 78 (2016) 135–143, https://doi.org/10.1007/s10971-015-3931-x
[30] V.M. Gaikwad, S.A. Acharya, Investigation of spin phonon coupling in $BiFeO_3$ based system by Fourier transform infrared spectroscopy, J. Appl. Phys. 114 (2013) 193901, https://doi.org/10.1063/1.4831676
[31] R. Bujakiewicz-Korońska, B. Ł. Hetmańczyk, A. Garbarz-Glos, J. Budziak, J. Koronski, M. Hetmańczyk, A. Antonova, D.Na.łęcz Kalvane, Investigations of low temperature phase transitions in $BiFeO_3$ ceramic by infrared spectroscopy, Ferroelectrics 417 (9) (2011) 63–69, https://doi.org/10.1080/00150193.2011.578495
[32] D. Voll, A. Beran, H. Schneider, Variation of infrared absorption spectra in the system $Bi_2Al_{4-x}Fe_xO_9$ (x = 0–4), structurally related to mullite, Phys. Chem. Minerals 33 (2006) 623–628, https://doi.org/10.1007/s00269-006-0108-8
[33] R.P.S.M. Lobo, R.L. Moreira, D. Lebeugle, D. Colson, Infrared phonon dynamics of a multiferroic $BiFeO_3$ single crystal, Phys. Rev. B 76 (2007) 172105, https://doi.org/10.1103/PhysRevB.76.172105
[34] D.M. Giaquinta, G.C. Papaefthymiou, W.M. Davis, H.C.R. Loye, Synthesis, structure, and magnetic properties of the layered bismuth transition metal oxide solid solution $Bi_2Fe_{4-x}Ga_xO_9$, J. Solid State Chem. 99 (1992) 120, https://doi.org/10.1016/0022-4596(92)90296-8
[35] D. Groult, M. Hervieu, N. Nguyen, B. Raveau, 3.1 GeV-xenon ion latent tracks in $Bi_2Fe_4O_9$: mössbauer and electron microscopy studies, J. Solid State Chem. 76 (1988) 248–259, https://doi.org/10.1016/0022-4596(88)90216-2
[36] P. Rovillain, M. Cazayous, A. Sacuto, D. Lebeugle, D. Colson, Piezoelectric measurements on $BiFeO_3$ single crystal by Raman scattering, JMMM 321 (2009) 1699–1701, https://doi.org/10.1016/j.jmmm.2009.02.020
[37] I. Sosnowska, T. Peterlin-Neumaier, E. Streichele, Spiral magnetic ordering in bismuth ferrite, J. Phys. C. 15 (1982) 4835–4846, https://doi.org/10.1088/0022-3719/15/23/020
[38] A.K. Pradhan, K. Zhang, D. Hunter, J.B. Dadson, G.B. Loutts, P. Bhattacharya, R. Katiyar, J. Zhang, D.J. Sellmyer, U.N. Roy, Y. Cui, A. Burger, Magnetic and electrical properties of single-phase multiferroic $BiFeO_3$, JAP 97 (2005) 093903, https://doi.org/10.1063/1.1881775
[39] V.R. Palkar, D.C. Kundaliya, S.K. Malik, S. Bhattacharya, Magnetoelectricity at room temperature in the $Bi_{0.9-x}Tb_xLa_{0.1}FeO_3$ system, Phys. Rev. B 69 (2004) 212102, https://doi.org/10.1103/PhysRevB.69.212102
[40] A.A. Amirov, A.B. Batdalov, S.N. Kallaev, Z.M. Omarov, I.A. Verbenko, O.N. Razumovskaya, L.A. Reznichenko, L.A. Shilkina, Features of thermal, magnetic and dielectric properties of $BiFeO_3$ and $Bi_{0.95}La_{0.05}FeO_3$ multiferroics, Solid Stat. Phys. 51 (2009) 1123–1126.
[41] Yilin Zhang, Yuhan Wang, Ji Qi, Yu Tian, Mingjie Sun, Junkai Zhang, Tingjing Hu, Maobin Wei, Yanqing Liu, Jinghai Yang, Enhanced magnetic properties of $BiFeO_3$ thin films by doping: analysis of structure and morphology, Nanomaterials 8 (2018) 711, https://doi.org/10.3390/nano8090711
[42] V.E. Dmitrienko, E.N. Ovchinnikova, S.P. Collins, G. Nisbet, G. Beutier, Y.O. Kvashnin, V.V. Mazurenko, A.I. Lichtenstein, M.I. Katsnelson, Measuring the Dzyaloshinskii–Moriya interaction in a weak ferromagnet, Nat. Phys. 10 (2014) 202–206 http://www.nature.com/doifinder/10.1038/nphys2859..
[43] S.T. Zhang, M.H. Lu, D. Wu, Y.F. Chen, N.B. Ming, Larger polarization and weak ferromagnetism in quenched $BiFeO_3$ ceramics with a distorted rhombohedral crystal structure, Appl. Phys. Lett. 87 (2005) 262907, https://doi.org/10.1063/1.2147719
[44] P. Dimple, Balaji Dutta, P. Mandal, Ratna Naik, Gavin Lawes, Avesh K. Tyagi, Magnetic, Ferroelectric and magnetocapacitive properties of sonochemically synthesized Sc-doped $BiFeO_3$ nanoparticles, J. Phys. Chem. C. 117 (2013) 2382–2389, https://doi.org/10.1021/jp310710p
[45] P. Rovillain, M. Cazayous, Y. Gallais, A. Sacuto, R.P.S.M. Lobo, D. Lebeugle, D. Colson, Polar phonons and spin excitations coupling in multiferroic $BiFeO_3$ crystals, 180411(R), Phys. Rev. B 79 (2009), https://doi.org/10.1103/PhysRevB.79.180411
[46] M. Cazayous, Y. Gallais, A. Sacuto, R. de Sousa, D. Lebeugle, D. Colson, Possible Observation of Cycloidal Electromagnons in $BiFeO_3$, Phys. Rev. Lett. 101 (2008) 037601, https://doi.org/10.1103/PhysRevLett.101.037601
[47] K.P. Belov, Magnetostrictive phenomena and their technical applications, Nauka, Moscow, 1987, p. 160.
[48] K.P. Belov, G.I. Kataev, R.Z. Levitin, S.A. Nikitin, V.I. Sokolov, Usp. Phys. Sci. 140 (1983) 271–313.
[49] M. Ramazanoglu, W. Ratcliff, H.T. Yi, A.A. Sirenko, S.-W. Cheong, V. Kiryukhink, Giant effect of uniaxial pressure on magnetic domain populations in multiferroic bismuth ferrite, PRL 107 (2011) 067203https://10.1103/PhysRevLett.107.067203..
[50] Alison J. Hatt, Nicola A. Spaldin, Claude Ederer, Strain-induced isosymmetric phase transition in $BiFeO_3$, Phys. Rev. B 81 (2010) 054109, https://doi.org/10.1103/PhysRevB.81.054109
[51] D. Kan Lucia Pa ´lova ´, Varatharajan Anbusathaiah, Ching Jung Cheng, Shigehiro Fujino, Valanoor Nagarajan, Karin M. Rabe, Ichiro Takeuchi, Universal behavior and electric-field-induced structural transition in rare-earth-substituted $BiFeO_3$, Adv. Funct. Mater. 20 (7) (2010) 1108, https://doi.org/10.1002/adfm.200902017